Applied Energy 120 (2014) 16–22

Contents lists available at ScienceDirect

Applied Energy

journal homepage: www.elsevier.com/locate/apenergy

Performance optimization analyses and parametric design criteria of a dye-sensitized solar cell thermoelectric hybrid device

Shanhe Su [a], Tie Liu [a], Yuan Wang [a], Xiaohang Chen [a], Jintong Wang [b], Jincan Chen [a,*]

[a] Fujian Key Laboratory of Semiconductor Materials and Applications and Department of Physics, Xiamen University, Xiamen 361005, People's Republic of China
[b] Department of Physics, Southern University, Baton Rouge, USA

HIGHLIGHTS

- An electric and thermal model of the solar hybrid device is studied.
- Temperature effects on the performance of a dye-sensitized solar cell are discussed.
- The performances of the solar cell and hybrid device are optimized and compared.
- The criteria of optimal coupling and parametric design are obtained.
- The hybrid device is proved to be an efficient system exploiting solar energy.

ARTICLE INFO

Article history:
Received 3 August 2013
Received in revised form 24 November 2013
Accepted 16 January 2014
Available online 7 February 2014

Keywords:
Dye-sensitized solar cell
Thermoelectric generator
Hybrid device
Temperature-dependent coefficient
Performance analysis
Optimum design strategy

ABSTRACT

An electric and thermal model of the hybrid device consisting of a dye-sensitized solar cell (DSSC) and a thermoelectric generator (TEG) is studied for exploiting the solar full spectrum. Analytical expressions for the power outputs and efficiencies of the DSSC, TEG and hybrid device are derived. Temperature-dependent coefficients of the DSSC are introduced and their values being consistent with the experimental data are determined. The effects of the operating electric current, working temperature and temperature-dependent coefficient in the DSSC on the performance of the hybrid device are discussed in detail. The optimum performance characteristics of the hybrid derive at different temperature conditions and the DSSC at the reference temperature condition are compared. The parametric design criteria of the optimal coupling are given. These results obtained here may provide some guidance for the optimum design of practical hybrid devices.

1. Introduction

The dye-sensitized solar cell (DSSC) has aroused considerable attention with the continuous growth of the advantages of its potential low cost, high solar energy conversion efficiency and increasing stability, since reported by O'Regan and Gratzel [1]. It has shown a potential as a new renewable energy device. In practice, the DSSC is expected to be applied in widespread fields ranging from Building-integrated photovoltaics to the mobile and hydrogen production due to its flexible, economical and high permeable properties [2–6].

Although the DSSC may possess many attractive advantages in comparison with currently existing silicon semi-conductive solar cells, only solar spectrum wavelength larger than 800 nm can be absorbed by the common used N3 and N719 sensitizers [7], and at the same time, relaxation, interfacial transference, and recombination process are the main factors governing the efficiency of energy conversion [8,9], so that irreversible losses in the device limit the performance of the cell. Various experimental and theoretical studies including the synthesis of new absorber materials [10,11], optimization of the metal oxides structure [12–14], application of tandem configuration [15,16], etc. have been carried out to improve the performance of the DSSC. However, few researches are concentrating on recycling the vast waste sunlight which mostly converts to heat. Until recently, several researchers [7] developed a novel hybrid system comprising a DSSC and a thermoelectric generator. Chang et al. used the integration of the CuO thin film to enhance the overall heat conduction [17]. Another system composed of a DSSC, a solar selective absorber, and a thermoelectric device is proved to possess the probability of effectively increasing the photoelectric conversion efficiency [18]. Most researches experimentally proved that the efficiency can be increased by using a hybrid system. Since it is difficult to

* Corresponding author.
E-mail address: jcchen@xmu.edu.cn (J. Chen).

0306-2619/$ - see front matter © 2014 Elsevier Ltd. All rights reserved.
http://dx.doi.org/10.1016/j.apenergy.2014.01.048

Nomenclature

A	effective area (cm)
d	thin film thickness (μm)
D	electron diffusion length ($cm^2\ s^{-1}$)
G	solar spectrum intensity (mW/cm^2)
h	overall heat leak coefficient ($mW/cm^2\ K$)
i	reduced current of the TEG
I	electric current of the TEG (mA)
J	current density of the DSSC (mA/cm^2)
k	thermal conductivity (mW/cm K)
K	thermal conductance (mW/K)
k_B	Boltzmann constant ($J\ K^{-1}$)
l	electron diffusion length (cm)
L	length of thermoelectric arms (cm)
m	couple number of the TEG
M	ideality factor
$n(x)$	excessive electron concentration (cm^{-3})
n_0	electron concentration under a dark condition (cm^{-3})
P	power output (mW)
q	electron charge (C)
Q_h	heat flow from DSSC to TEG (mW)
Q_c	heat flow from TEG to the heat sink (mW)
Q_L	heat leak rate (mW)
S	Seebeck coefficient (V/K)
T	temperature (K)
T_a	temperature of the heat sink/environment (K)
$T_{H/L}$	two temperatures of the hybrid device (K)
V	external voltage of the DSSC (V)
x	coordinate measured from the TiO_2/TCO interface (μm)
Z	figure of merit (K^{-1})

Greek symbols

α	light absorption coefficient (cm^{-1})
β	decreasing rate of the efficiency (K^{-1})
β_0	decreasing rate of the efficiency when the maximum efficiency of the hybrid device is equal to that of the DSSC at the reference temperature condition (K^{-1})
ρ	electrical resistivity (Ω cm)
λ	decreasing rate of the power output ($mW\ K^{-1}$)
η_{opt}	optical efficiency
η	efficiency
Φ	incident irradiation intensity ($cm^{-2}\ s^{-1}$)
Φ_0	light intensity at 1 sun condition ($cm^{-2}\ s^{-1}$)
τ	electron lifetime (ms)

Superscripts and subscripts

D	dye-sensitized solar cell
T	thermoelectric generator
opt	optimal value
n	N-type semiconductor leg
p	P-type semiconductor leg
sc	short-circuit current density
ref	reference condition
oc	open circuit

Abbreviations

DSSC	dye-sensitized solar cell
TEG	thermoelectric generator
TCO	transparent conducting oxide

experimentally quantify the interrelated parameters governing a hybrid system, theoretical modeling and numerical analysis become essential for the optimization of operating conditions and the system design. Therefore, the motivation of the present paper is to clarify these issues and present a general and fundamental analysis of the performance characteristics of the DSSC, TEG, and hybrid system.

In the present paper, an electric and thermal model is established based on two existing models of a DSSC and a semiconductor thermoelectric generator. Temperature coefficient is introduced to determine the electrical performance of the DSSC depending on temperature. Expressions for the power output and efficiency of the hybrid device are derived. To make the hybrid system more competitive, a numerical optimization method is developed for evaluating the performance of the each component and total system. The effects of the operating electric current, working temperature, and temperature-dependent coefficients of the DSSC on the performance of the system are discussed in detail. The efficiency of the hybrid device is maximized at differently given conditions. The optimal criteria of the parametric design are obtained.

2. The description of a photovoltaic–thermoelectric hybrid device

The photovoltaic–thermoelectric hybrid device shown in Fig. 1 consists of a series-connected DSSC on the top and a series-connected semiconductor thermoelectric generator attached to the back side of the cell. When a ray of sun light incidents on the DSSC, it is partly lost by transmission and reflection. The rest light energy is selectively absorbed by optical active substances such as the sensitized molecular in the DSSC and the solar absorber material coated on the bottom of the DSSC [7]. One part of the absorbed energy is directly converted to electric and transported to the load. The remaining part of the absorbed energy converts into heat, which may be used to drive a TEG. By using such a hybrid device, the solar spectrum with all frequencies can be better utilized and converted to electricity. Below, the thermal and electrical performance evolution of individual unit and overall system will be given.

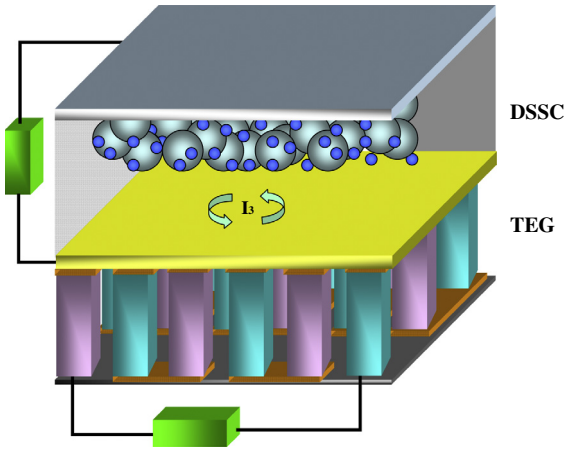

Fig. 1. The schematic diagram of a DSSC–TEG hybrid device.

2.1. The power output and efficiency of a DSSC

Structure and operation of a DSSC have been extensively studied [1,9,19–27]. Under solar radiation, electrons of the dye molecule in the DSSC are excited by large energy photons, subsequently injected into the conduction band of the semiconductor thin film. For a semiconductor thin film composed of TiO_2, it is theoretically predicted that the electron transfer in TiO_2 is mainly driven by diffusion [19,20]. A nanoporous TiO_2 film can be prepared by spreading a viscous dispersion of colloidal TiO_2 particles on a conducting glass support following the methods described by Nazeeruddin et al. [21]. By soaking the TiO_2 film for hours in a solution of the ruthenium complex in dry ethanol, dye molecules will be well distributed on the surface of TiO_2. The counter electrode materials can be metals such as platinum, gold and nickel, various nanostructured carbon materials, and conductive polymers. The counter electrode is directly placed on top of the dye-coated TiO_2 film, supported by the conducting glass sheet. After encountering the transparent conducting oxide (TCO) electrode, electrons flow through the external circuit and reach the counter electrode. The original dye molecular will be regenerated by the electrons donated from the counter electrolyte, which usually applies to a redox system [22,23]. A redox couple, as one of the important components of the DSSC, is used to regenerate the oxidized dye molecules and to carry positive charge to the counter electrode. In addition, free carriers during transportation have the possibility to be captured by recombination processes, which lead to the decrease of the efficiency [9]. Based on the assumptions that the charge carrier transport in the semiconductor occurs via diffusion and the diffusion length is constant, the generation, transport, and recombination of electrons within the DSSC film under steady-state conditions can be described by the following differential equation [19,20,24–26]:

$$D\frac{\partial^2 n(x)}{\partial x^2}-\frac{n(x)-n_0}{\tau}+\Phi\alpha e^{-\alpha x}=0 \tag{1}$$

where x is the coordinate measured from the TiO_2/TCO interface, $n(x)$ is the excessive electron concentration at x, n_0 is the electron concentration under a dark condition, D is the electron diffusion length, τ is the electron lifetime, $\Phi=\Phi_0\eta_{opt}$ is the incident irradiation intensity considering the transmission and reflection loss, Φ_0 is the light intensity at 1 sun condition ($G=100\ \mathrm{mW/cm^2}$), η_{opt} is the optical efficiency of the glass cover, and α is the light absorption coefficient of the porous electrode.

Under illumination, the external voltage V of the DSSC is regarded as the difference between the Fermi level of the electrons in the semiconductor TiO_2 film and the redox electrochemical potential [22,23]. Considering the boundary condition of the operating DSSC ($n(0)=n$ and $\left(\frac{dn}{dx}\right)_{x=d}=0$), one can solve Eq. (1) to obtain the J–V relationship as [24–26]

$$V=\frac{k_BT_{ref}M}{q}\ln\left[\frac{l(J_{SC}-J)}{qDn_0\tanh\left(\frac{d}{l}\right)}+1\right] \tag{2}$$

where

$$J_{SC}=\frac{q\Phi l\alpha}{1-l^2\alpha^2}\left[-l\alpha+\tanh\left(\frac{d}{l}\right)+\frac{l\alpha\exp(-d\alpha)}{\cosh\left(\frac{d}{l}\right)}\right] \tag{3}$$

is the short-circuit current density depending on the short-circuit boundary conditions $n(0)=n_0$ and $\left(\frac{dn}{dx}\right)_{x=d}=0$, M is the ideality factor, $l=\sqrt{D\tau}$ is the electron diffusion length, k_B is the Boltzmann constant, q is the charge of an electron, d is the thin film thickness, T_{ref} is the operating temperature at the reference condition, and J is the current density of the DSSC.

From Eqs. (1) and (2), one can derive the power output and efficiency of the DSSC as

$$P_{D,ref}=VJA_D=\frac{k_BT_{ref}M}{q}JA_D\ln\left[\frac{l(J_{SC}-J)}{qDn_0\tanh\left(\frac{d}{l}\right)}+1\right] \tag{4}$$

and

$$\eta_{D,ref}=\frac{P_{D,ref}}{GA_D}=\frac{k_BT_{ref}M}{Gq}J\ln\left[\frac{l(J_{SC}-J)}{qDn_0\tanh\left(\frac{d}{l}\right)}+1\right], \tag{5}$$

where G is the solar spectrum intensity and A_D is the effective area of the DSSC under illumination.

It has been experimentally confirmed [28–32] that the operating temperature has a great influence on the photoelectric conversion efficiency of the DSSC, because the diffusion and recombination reactions of the interior structure in the DSSC are quite sensitive to the change of temperature. In Berginic's study, the open circuit voltage V_{OC} is a linear decrease function of the operating temperature, but it is different for the short circuit current I_{SC} [28]. The power output decreases when the cell temperature increases [29,30]. The authors in Ref. [31] studied the temperature dependent effects on the performance of the DSSC and found that all the cells have the lowest efficiency at 70 °C, indicating more disadvantageous such as activation-triggered effects and increased recombination taking place at the higher temperatures. The temperature effect [32] is considered in a DSSC module connected to an adaptable power conditioning system. The I–V characteristics obtained in Ref. [32] show that the current is almost constant and the voltage decreases when the temperature increases. At the reference temperature T_{ref}, the performance of the DSSC can be simulated and explained by Eqs. (4) and (5). But Eqs. (4) and (5) are insufficient for explaining the temperature effects on the performance of the DSSC. In order to describe the deviations of the power output and efficiency from the ones at the reference temperature condition, the following equations

$$P_D=P_{ref}-\lambda(T-T_{ref}) \tag{6}$$

and

$$\eta_D=\eta_{D,ref}[1-\beta(T-T_{ref})] \tag{7}$$

are often used [33,34], where λ and β are the decreasing rate of the power output and efficiency as the operating temperature T increases and are dependent on each other. It is found that when $\lambda=0.00506\ \mathrm{mW\,K^{-1}}$, the curve of the maximum power output of the DSSC fits well with the experimental data obtained in Ref. [29], as shown in Fig. 2. According to Eqs. (4)–(7), one can calculate $\beta=0.0278\ \mathrm{K^{-1}}$ when $\lambda=0.00506\ \mathrm{mW\,K^{-1}}$. Substituting Eqs. (4) and (5) into Eqs. (6) and (7), one has

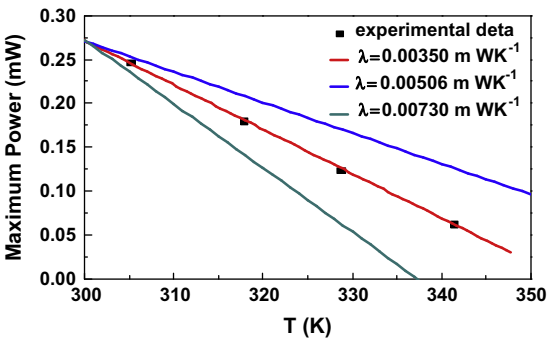

Fig. 2. Curves of the maximum power of the DSSC varying with operating temperature.

$$P_D = \frac{k_B T_{ref} M}{q} J A_D \ln\left[\frac{l(J_{SC}-J)}{qDn_0 \tanh\left(\frac{d}{l}\right)} + 1\right] - \lambda(T - T_{ref}) \quad (8)$$

and

$$\eta_D = \frac{k_B T_{ref} M}{Gq} J \ln\left[\frac{l(J_{SC}-J)}{qDn_0 \tanh\left(\frac{d}{l}\right)} + 1\right][1 - \beta(T - T_{ref})] \quad (9)$$

which can be used to describe the performance of the DSSC varying with the operating temperature.

2.2. The power output and efficiency of a thermoelectric generator

It is well known that a semiconductor thermoelectric generator can directly convert a part of the absorbed heat into electricity. Practical device contains a number of N- and P-type semiconductor legs connected electrically in series and thermally in parallel, as shown in Fig. 1. It is often assumed that the Seebeck coefficient S, the electrical resistivity ρ and the thermal conductivity k are independent of temperature [35]. It has been proved that when the relation $L_n A_p/(L_p A_n) = [k_n \rho_p/(k_p \rho_n)]^{1/2}$ is satisfied, the figure of merit of the TEG attains its maximum [36,37], i.e., $Z = (S_p - S_n)^2/[(k_p\rho_p)^{1/2} + (k_n\rho_n)^{1/2}]^2 \equiv Z_{max}$, where A and L are the cross-sectional area and length of the thermoelectric arms, and the subscripts n and p represent the N- and P-type semiconductor legs, respectively.

According to Fig. 1 and the results derived in Ref. [36], the heats absorbed from the heat source and released to the heat sink per unit time can be, respectively, expressed as [36,37]

$$Q_h = K[Ti - i^2/(2Z) + T - T_a] \quad (10)$$

and

$$Q_c = K[T_a i + i^2/(2Z) + T - T_a] \quad (11)$$

where $K = [k_p + (k_n k_p \rho_n/\rho_p)^{1/2}]mA_p/L_p$, $i = SI/K$, I is the electric current of the TEG, and m is the couple number of the TEG, T_a is the temperature of the heat sink. Using Eqs. (10) and (11), we can derive the power output P_T and efficiency η_T of the TEG as

$$P_T = KT_a\left[\left(\frac{T}{T_a} - 1\right)i - \frac{i^2}{ZT_a}\right] \quad (12)$$

and

$$\eta_T = \frac{Z(T - T_a)i - i^2}{ZiT - \frac{1}{2}i^2 + Z(T - T_a)} \quad (13)$$

From Eqs. (12), it is easily found that only when $0 < i < Z(T - T_a)$ can the thermoelectric device works as a generator.

2.3. The power output and efficiency of a hybrid device

According to Fig. 1, one part of the heat produced in the DSSC is transferred to the TEG on the bottom of the DSSC and the other part is directly released to the environment from the front surface, which is called the external heat leak of the DSSC. The heat leak may be simply determined by

$$Q_L = hA_D(T - T_a), \quad (14)$$

where h is the overall heat leak coefficient and is considered by the convection between the DSSC and the environment. Assuming the overall convective heat transfer is controlled by the forced convection from the front surface, h is taken to be 0.28 mW/(cm^2 K) while the average wind speed is regarded as zero to lower the heat loss by convection [38,39]

According to the first law of thermodynamics, the input heat from the DSSC to the TEG is

$$Q_h = \eta_{opt} G A_D - P_D - Q_L. \quad (15)$$

By using Eq. (15) and the data in Tables 1 [40–43] and 2 [39], we can generate the curves of the reduced current i in the TEG varying with the current density J in the DSSC, as shown in Fig. 3, where $\beta = 0.00501$ K^{-1} and the structure parameter of the hybrid system $mA_p/(A_D L_p) = 0.0420$ cm^{-1}. It is seen from Fig. 3 that the current i is not a monotonic function of the current J for given temperatures. When J increases, the efficiency η_D of the DSSC increases, and consequently, the less heat releases to the TEG, resulting in the decrease of i. However, after η_D reaches the maximum, the further increase of J will lead to the release of the more heat to the TEG and the increase of i. In addition, it should be noted that when the temperature increases, the current i decreases and the operating range $Z(T - T_a)$ of the current in the TEG increases. It implies the fact that when the temperature is low, the current i will be larger than $Z(T - T_a)$, so that the thermoelectric device cannot work as a generator.

By using Eqs. 8, 9, and 12, the power output and efficiency of the hybrid device can be, respectively, expressed as

$$\begin{aligned} P &= P_D + P_T \\ &= \frac{k_B T_{ref} M}{q} J A_D \ln\left[\frac{l(J_{SC}-J)}{qDn_0 \tanh\left(\frac{d}{l}\right)} + 1\right] - \lambda(T - T_{ref}) \\ &\quad + KT_a\left[\left(\frac{T}{T_a} - 1\right)i - \frac{i^2}{ZT_a}\right] \end{aligned} \quad (16)$$

and

$$\eta = \frac{P}{GA_D} = \eta_D + \frac{K}{GA_D}\left[(T - T_a)i - \frac{i^2}{Z}\right]. \quad (17)$$

Obviously, the efficiency of the hybrid device is proportional to the power output of the hybrid device for a given GA_D. Thus, it is sufficient to calculate the efficiency or power output of the hybrid device under the following discussion.

3. Performance evaluation

Using Eqs. 9, 13, 15, and 17 and the data in Tables 1 and 2, one can generate three-dimensional graphs of the efficiencies of the DSSC η_D, TEG η_T, and hybrid device η varying with the current density J and the working temperature T of the DSSC, as shown in Fig. 4. According to Fig. 4(a), a suitable current density J can be found to obtain the maximum efficiency of the DSSC, but the efficiency of the DSSC is a monotonically decreasing function of the working temperature. The maximum efficiency of the DSSC obtained in the condition is 4.26% when the current density J is equal to 11.4 mA/cm^2. Temperature is likely to influence the recombination, dye absorption/desorption, ionic mobility, diffusion, and conductivity [44]. The lower efficiencies for the cell at higher temperatures indicate that more disadvantageous, most likely recombination, and irreversible chemical effect start to take place [31]. As the temperature further increases, the efficiency of the DSSC may close to zero. Therefore, a hybrid system should be introduced to further utilize the solar radiation. For a thermoelectric generator, the temperature has a significant effect on the efficiency η_T, as shown in Fig. 4(b). When $Z(T - T_a) \leqslant i$, the thermoelectric device cannot work as a generator. The TEG starts to work only when temperature increases and $Z(T - T_a) > i$ is satisfied. The efficiency of the TEG increases with the increase of the temperature and attains its maximum. But, the further increase of the temperature will result in an opposite result. Thus, an appropriate working temperature should be determined to get the maximum efficiency η_T. The TEG alone can recover 1.57% of the waste heat. For given materials, the conversion efficiency has the potential to be improved if the

Table 1
Parameters used in a DSSC modeling analysis [40–43].

Parameters	Symbol	Numerical value
Optical efficiency	η_{opt}	0.970
Incident irradiation intensity under 1 sun condition	Φ_0	1.00×10^{17} cm^{-2} s^{-1} [27,42]
Light absorption coefficient	α	5.00×10^{3} cm^{-1} [27,42]
Electron concentration under a dark condition	n_0	1.00×10^{16} cm^{-3} [40,41]
Thin film thickness	d	10.0 μm
Ideality factor	M	4.50 [27,42]
Electron diffusion length	l	2.24×10^{-3} cm
Electron lifetime	τ	10.0 ms [42,43]
Electron diffusion coefficient	D	5.00×10^{-4} cm^2 s^{-1} [25]
Elementary electron charge	q	1.60×10^{-19} C
Boltzmann constant	k_B	1.38×10^{-23} J K^{-1}
1 Sun condition	G	100 mW/cm^2
Environment/reference temperature	T_a/T_{ref}	300 K

Table 2
Parameters of the thermoelectric materials [39].

Type	S (V/K)	ρ (Ω cm)	κ (mW/cm K)
N_1	-2.12×10^{-4}	1.30×10^{-3}	14.5
N_2	-2.31×10^{-4}	4.05×10^{-3}	13.4
P_1	1.59×10^{-4}	0.740×10^{-3}	18.6
P_2	2.26×10^{-4}	0.360×10^{-3}	12.6

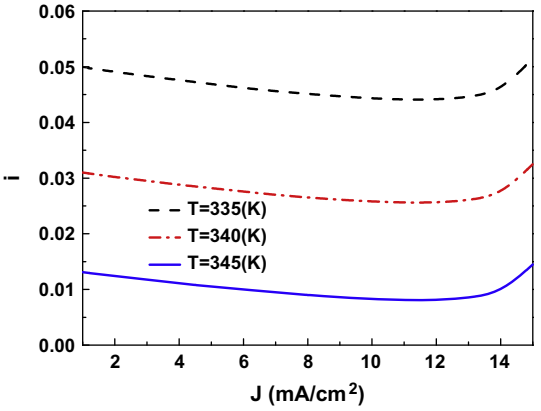

Fig. 3. Curves of the reduced current i of the TEG varying with the current density J of the DSSC at different temperatures, where $\beta = 0.00501$ K^{-1} and $mA_P/(A_D L_P) = 0.0420$ cm^{-1} .

structure parameters of the TEG are optimally selected. Fig. 4(c) shows the efficiency graph of the hybrid system, which is separated into two parts. At lower temperatures, only the DSSC is effectively operated. As the temperature increases, the efficiency of the DSSC decreases. When the condition $0 < i < Z(T - T_a)$ is satisfied, the thermoelectric device begins to work as a generator with the power output. When the temperature rises to a certain value, the efficiency of the hybrid device attains its maximum and is larger than the efficiency of the DSSC at the reference temperature condition. When the temperature further increases, the efficiency of the hybrid device decreases. It means that there exists an optimally working temperature for the DSSC. Fig. 4(c) also shows that the efficiency of the hybrid device is not a monotonic function of J and there exists an optimal value for J so that the efficiency of the hybrid device attains its maximum. The conversion efficiency of the hybrid system can arrive at 4.71% when the current density and the working temperature for the DSSC are, respectively, 11.5 mA/cm^2 and 338 K. In order to reveal how the conversion efficiency of the DSSC is further enhanced by using a hybrid system, the optimum problem of the parametric design will be discussed in the next sections.

4. Optimal coupling criteria

Using Eqs. 5, 7, and 17, we can continue to discuss the effect of the temperature coefficient β of the DSSC on the efficiency of the hybrid device, as shown in Fig. 5. It is seen from the curves in Fig. 5 that the efficiency of the hybrid device decreases with the increase of β. When $\beta = \beta_0$, which is referred to as the critical value of β, the maximum efficiency of the hybrid device is equal to that of the DSSC at the reference temperature condition. When $\beta > \beta_0$, the maximum efficiency of the hybrid device is smaller than that of the DSSC, and consequently, the hybrid device has lost its practical meaning. In such a case, one should exert every effort to increase the heat-transfer area between the DSSC and the environment

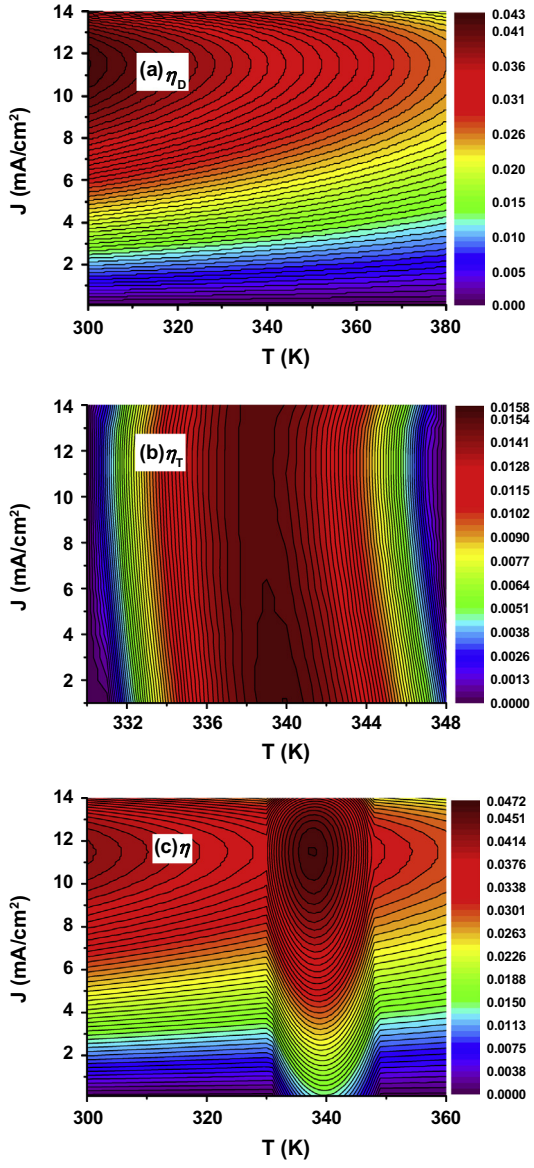

Fig. 4. Three-dimensional graphs of the efficiency of (a) the DSSC, (b) TEG, and (c) hybrid device varying with the current density J and the working temperature T of the DSSC. The values of the relevant parameters are the same as those used in Fig. 3.

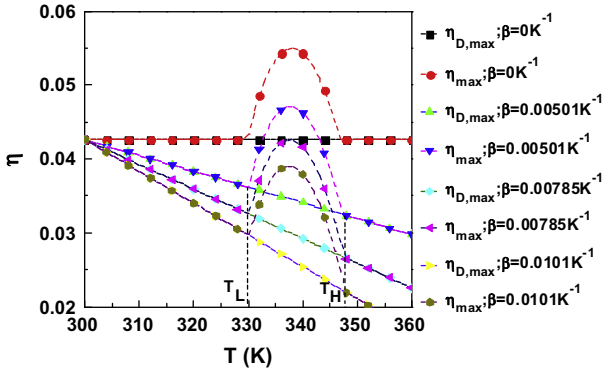

Fig. 5. Curves of the maximum efficiency η_{max} of the hybrid system varying with temperature of the DSSC for given values of β, where the horizontal line indicates the efficiency of the DSSC at the reference temperature condition. T_L and T_H are two operating temperatures of the hybrid device when the efficiency of the hybrid device is equal to that of the DSSC. The values of the relevant parameters are the same as those used in Fig. 3.

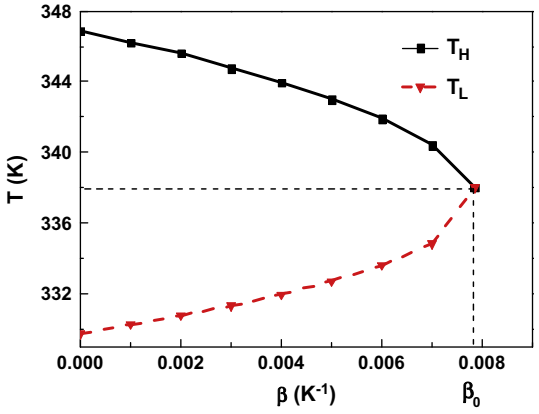

Fig. 6. Curves of the temperatures T_L and T_H varying with the temperature coefficient β.

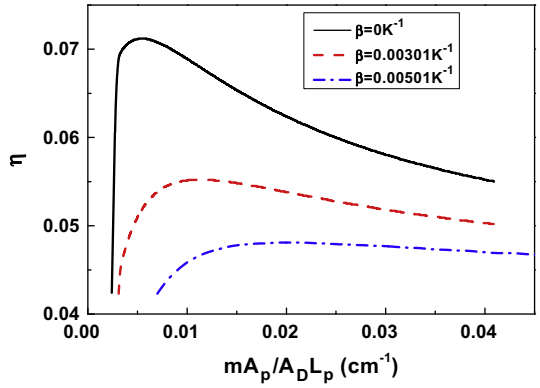

Fig. 7. Curves of the optimized efficiency varying with the structure parameter $mA_p/(A_DL_p)$.

and to lower the temperature of the DSSC to the environmental temperature as much as possible, so that the DSSC can obtain a large efficiency. When $\beta < \beta_0$ and $T = T_L$ or $T = T_H$, the efficiency of the hybrid device is equal to that of the DSSC. Obviously, the values of T_L and T_H are closely dependent on the value of β, as shown in Fig. 6. Fig. 5 shows that when $\beta < \beta_0$ and the temperature of the DSSC is at the range of $T_L < T < T_H$, the efficiency of the hybrid device will be larger than that of the DSSC. When β increases, the temperature range $\Delta = T_H - T_L$ diminishes. When $\beta = \beta_0$, $T_H = T_L$. According to the analyses above, we obtain two important criteria of the optimal design for hybrid devices as

$$\beta < \beta_0 \tag{18}$$

and

$$T_L < T < T_H. \tag{19}$$

When the two criteria are satisfied, the application of the hybrid device can efficiently improve the conversion efficiency of solar energy.

5. Parametric optimum design

Using Eq. (17), we can further discuss the effect of the structure parameter $mA_p/(A_DL_p)$ of the hybrid device on the efficiency, as shown in Fig. 7, where the efficiency η has been optimized with respect to the parameters T and J. It is seen from Fig. 7 that there exists an optimal structure parameter so that the efficiency of the hybrid device attains its maximum η_{max}. Using Eq. (17), we can calculate the maximum efficiencies of the hybrid device for given values of β and the optimal values of other main parameters at the maximum efficiency. The data obtained are listed in Table 3. By using the coating of a CuO thin film onto the TEG surface coated on the bottom of the DSSC in Ref. [17], the exhaust heat can be recycled more efficiently to generate additional electric power to enhance the overall solar energy conversion efficiency. The experimental results show that this solar-thermoelectric module can generate about 4.95 mW/cm^2 under the same solar radiation intensity. It is found in this paper that the maximum conversion efficiency larger than 4.50% can be obtained when the temperature coefficient β is smaller than 0.00501. The performance can be further improved if the operating electric current, working temperature, and structure parameter of the DSSC are optimally designed.

The results obtained here demonstrate that the DSSC–TEG hybrid system can effectively increase the photoelectric conversion efficiency of a DSSC and is a promising configuration for realizing high solar energy conversion efficiencies. Meanwhile, there is still a large room for further improvement in the performance of this

Table 3
The maximum efficiencies of the hybrid device for differently given values of β and the optimal values of other main parameters at the maximum efficiency.

β (K^{-1})	η_{max}	$\eta_{D,opt}$	$\eta_{T,opt}$	$[mA_p/(A_DL_p)]_{opt}$ (cm^{-1})	T_{opt} (K)	i_{opt}
0	0.0730	0.0443	0.0593	0.00542	458	0.148
0.00101	0.0667	0.0443	0.0545	0.00663	444	0.129
0.00201	0.0612	0.0443	0.0463	0.00905	421	0.107
0.00301	0.0565	0.0443	0.0402	0.0115	404	0.0939
0.00401	0.0525	0.0443	0.0302	0.0175	377	0.0700
0.00501	0.0493	0.0443	0.0275	0.0199	370	0.0633
0.00561	0.0478	0.0443	0.0214	0.0272	354	0.0517
0.00601	0.0469	0.0443	0.0183	0.0333	346	0.0423
0.00661	0.0458	0.0443	0.0140	0.0454	335	0.0328
0.00701	0.0453	0.0443	0.0121	0.0538	330	0.0282

hybrid system by further optimization. Future experimental works would be conducted to quantitatively verify the present model. Dye molecules need to be further studied for alleviating temperature effects on the performance of the DSSC. The experimental methods described in Refs. [21,43] will be used to prepare the photoelectrode film, and then a solar selective absorber will be placed in between the DSSC and the TEG. For a thermoelectric generator, Bi_2Te_3 material can be used because of its excellent performance at the low temperature range. With illumination, the *J–V* characteristics of the hybrid system will be measured and quantitatively compared with the theoretical results.

6. Conclusions

An electric and thermal model of the hybrid device consisting of a DSSC and a semiconductor thermoelectric generator is established. The maximum efficiency of the hybrid device is calculated and the optimally working states of the hybrid device are determined. Temperature effects on the performance of the DSSC and hybrid device are analyzed in detail and compared. The optimum criteria of the parametric design are obtained. These results obtained here may provide some guidance for the optimum design of practical DSSC–TEG hybrid devices.

Acknowledgments

This work has been supported by the National Natural Science Foundation (No. 11175148), 973 Program (No. 2012CB619301), and the Fujian Natural Science Foundation (No. 2012J05097), People's Republic of China.

References

[1] O'regan B, Grätzel M. A low-cost, high-efficiency solar cell based on dye-sensitized. Nature 1991;353:737–40.
[2] Liu Y, Wang H, Shen H, Chen W. The 3-dimensional dye-sensitized solar cell and module based on all titanium substrates. Appl Energy 2010;87:436–41.
[3] Grätzel M. Photovoltaic and photoelectrochemical conversion of solar energy. Phil Trans R Soc A 2007;365:993–1005.
[4] Grätzel M. Mesoscopic solar cells for electricity and hydrogen production from sunlight. Chem Lett 2005;34:8–13.
[5] Li M, Liu Y, Wang H, Shen H. Synthesis of TiO_2 submicro-rings and their application in dye-sensitized solar cell. Appl Energy 2011;88:825–30.
[6] McConnell RD. Assessment of the dye-sensitized solar cell. Renew Sust Energy Rev 2002;6:273–95.
[7] Guo XZ, Zhang YD, Qin D, Luo YH, Li DM, Pang YT, et al. Hybrid tandem solar cell for concurrently converting light and heat energy with utilization of full solar spectrum. J Power Sources 2010;195:7684–90.
[8] Bisquert J, Vikhrenko VS. Interpretation of the time constants measured by kinetic techniques in nanostructured semiconductor electrodes and dye-sensitized solar cells. J Phys Chem B 2004;108:2313–22.
[9] Bisquert J, Fabregat-Santiago F, Kalyanasundaram K. Dye-sensitized solar cells. Boca Raton: CRC Press; 2010.
[10] Horiuchi T, Miura H, Sumioka K, Uchida S. High efficiency of dye-sensitized solar cells based on metal-free indoline dyes. J Am Chem Soc 2004;126:12218–9.
[11] Zhang W, Zhu R, Liu B, Ramakrishna S. High-performance hybrid solar cells employing metal-free organic dye modified TiO_2 as photoelectrode. Appl Energy 2012;90:305–8.
[12] Wang X, Li H, Liu Y, Zhao W, Liang C, Huang H, et al. Hydrothermal synthesis of well-aligned hierarchical TiO_2 tubular macrochannel arrays with large surface area for high performance dye-sensitized solar cells. Appl Energy 2012;99:198–205.
[13] Kang HY, Wang HP. Cu@C dispersed TiO_2 for dye-sensitized solar cell photoanodes. Appl Energy 2012;100:144–7.
[14] Meng QB, Takahashi K, Zhang XT, Sutanto I, Rao TN, Sato O, et al. Fabrication of an efficient solid-state dye-sensitized solar cell. Langmuir 2003;19:3572–4.
[15] Jeong WS, Lee JW, Jung S, Yun JH, Park NG. Evaluation of external quantum efficiency of a 12.35% tandem solar cell comprising dye-sensitized and CIGS solar cells. Sol Energy Mater Sol C 2011;95:3419–23.
[16] Ahn KS, Yoo SJ, Kang MS, Lee JW, Sung YE. Tandem dye-sensitized solar cell-powered electrochromic devices for the photovoltaic-powered smart window. J Power Sources 2007;168:533–6.
[17] Chang H, Kao M, Cho K, Chen S, Chu K, Chen C. Integration of CuO thin films and dye-sensitized solar cells for thermoelectric generators. Curr Appl Phys 2011;11:S19–22.
[18] Wang N, Han L, He H, Parkb NH, Koumoto K. A novel high-performance photovoltaic-thermoelectric hybrid device. Energy Environ Sci 2011;4:3676–9.
[19] Södergren S, Hagfeldt A, Olsson J, Lindquist SE. Theoretical models for the action spectrum and the current–voltage characteristics of microporous semiconductor films in photoelectrochemical cells. J Phys Chem 1994;98:5552–6.
[20] Gómez R, Salvador P. Photovoltage dependence on film thickness and type of illumination in nanoporous thin film electrodes according to a simple diffusion model. Sol Energy Mater Sol C 2005;88:377–88.
[21] Nazeeruddin MK, Kay A, Rodicio I, Humphry-Baker R, Mueller E, Liska P, et al. Conversion of light to electricity by cis-X_2bis (2,2′-bipyridyl-4,4′-dicarboxylate) ruthenium(II) charge-transfer sensitizers (X = Cl^-, Br^-, I^-, CN^-, and SCN^-) on nanocrystalline titanium dioxide electrodes. J Am Chem Soc 1993;115:6382–90.
[22] Grätzel M. Dye-sensitized solar cells. J Photochem Photobiol C 2003;4:145–53.
[23] Grätzel M. Conversion of sunlight to electric power by nanocrystalline dye-sensitized solar cells. J Photochem Photobiol A 2004;164:3–14.
[24] Ni M, Leung MKH, Leung DYC, Sumathy K. An analytical study of the porosity effect on dye-sensitized solar cell performance. Sol Energy Mater Sol C 2006;90:1331–44.
[25] Ni M, Leung MKH, Leung DYC, Sumathy K. Theoretical modeling of TiO_2/TCO interfacial effect on dye-sensitized solar cell performance. Sol Energy Mater Sol C 2006;90:2000–9.
[26] Ni M, Leung MKH, Leung DYC. Theoretical modelling of the electrode thickness effect on maximum power point of dye-sensitized solar cell. Can J Chem Eng 2008;86:35–42.
[27] Lee JJ, Coia GM, Lewis NS. Current density versus potential characteristics of dye-sensitized nanostructured semiconductor photoelectrodes. 2. Simulation. J Phys Chem B 2004;108:5282–93.
[28] Berginc M, Opara Krašovec U, Jankovec M, Topič M. The effect of temperature on the performance of dye-sensitized solar cells based on a propyl-methyl-imidazolium iodide electroly. Sol Energy Mater Sol C 2007;91:821–8.
[29] Ting CC, Chao WS. Measuring temperature dependence of photoelectric conversion efficiency with dye-sensitized solar cells. Measurement 2010;43:1623–7.
[30] Sebastián PJ, Oleac A, Campos J, Toledob JA, Gamboa SA. Temperature dependence and the oscillatory behavior of the opto-electronic properties of a dye-sensitized nanocrystalline TiO_2 solar cell. Sol Energy Mater Sol C 2004;81:349–61.
[31] Toivola M, Peltokorpi L, Halme J, Lund P. Regenerative effects by temperature variations in dye-sensitized solar cells. Sol Energy Mater Sol C 2007;91:1733–42.
[32] Lee KJ, Kim JH, Kim HS, Shin D, Yoo D, Kim H. A study on a solar simulator for dye sensitized solar cells. Int J Photoenergy 2012;2012:834347.
[33] Skoplaki E, Palyvos JA. On the temperature dependence of photovoltaic module electrical performance: a review of efficiency/power correlations. Sol Energy 2009;83:614–24.
[34] Perlman J, McNamara A, Strobino D. Analysis of PV system performance versus modelled expectations across a set of identical PV systems. In: Proc ISES Sol World Cong. "Bringing Water to the World, August 6–12, Orlando, Florida; 2005.
[35] Goldsmid HJ. Introduction to thermoelectricity. Verlag Berlin, Heidelberg: Springer; 2010.
[36] Chen J, Lin B, Wang H, Lin G. Optimal design of a multi-couple thermoelectric generator. Semicond Sci Technol 2000;15:184–8.
[37] Chen X, Chen L, Guo J, Chen J. An available method exploiting the waste heat in a proton exchange membrane fuel cell system. Int J Hydrogen Energy 2011;36:6099–104.
[38] Chow TT, He W, Ji J. Hybrid photovoltaic-thermosyphon water heating system for residential application. Sol Energy 2006;36:298–306.
[39] Rowe DM. Handbook of thermoelectrics: macro to nano. Boca Raton: CRC; 2005.
[40] Rothenberger G, Fitzmaurice D, Gratzel M. Spectroscopy of conduction-band electrons in transparent metal-oxide semiconductor-films: optical determination of the flat-band potential of colloidal titanium-dioxide films. J Phys Chem 1992;96:5983–6.
[41] Ferber J, Luther J. Modeling of photovoltage and photocurrent in dye-sensitized titanium dioxide solar cells. J Phys Chem B 2001;105:4895–903.
[42] Gomez R, Salvador P. Photovoltage dependence on film thickness and type of illumination in nanoporous thin film electrodes according to a simple diffusion model. Sol Energy Mater Sol C 2005;88:377–88.
[43] Dloczik L, Ileperuma O, Lauermann I, Peter LM, Ponomarev EA, Redmond G, et al. Dynamic response of dye-sensitized nanocrystalline solar cells: characterization by intensity modulated photocurrent spectroscopy. J Phys Chem B 1997;101:10281–9.
[44] Atkins PW. Physical chemistry. 5th ed. Oxford, Melbourne, Tokyo: Oxford University Press; 1994.